JOURNAL OF MATERIALS SCIENCE **37** (2002) 3005 – 3022

Effects of crystallinity, transcrystallinity and crystal phases of GF/PA on friction and wear mechanisms

H. C. Y. CARTLEDGE
Department of Mechanical and Mechatronic Engineering, University of Sydney NSW 2006 Australia
E-mail: helen.cartledge@dsto.defence.gov.au

C. A. BAILLIE
Department of Materials, Imperial College of Science, Technology and Medicine, Prince Consort Road, London SW7 2BP, UK
E-mail: c.baillie@ac.ic.uk

Relationships between manufacturing processes, microstructures, mechanical and tribological properties of GF/PA6 composite were revealed in this paper by experimental investigations and theoretical analysis. The study indicated that the wear resistance was significantly influenced by the thermal history of the composite. Decreasing cooling rate during the components thermal moulding would result in enhancing approximate 28% of wear resistance and reducing almost 14% of friction in the GF/PA6 composites. A slow cooling gives the PA6 a high crystallinity and high ratio of α/γ phases which resulted in higher thermal stabilities, higher density and harder matrix in the composites than that of fast cooling. It also improves the interfacial properties and the composite hardness. Due to the thermal decomposition, abrasion and adhesion dominated the wear mechanisms, these improvements led to a higher wear resistance and higher *pv* service limit in the slow cooled GF/PA6 samples than that of fast cooled samples. Interfacial debonding dominated the friction mechanisms in the unlubricated pin-on-disk tests. A poor interfacial bond led to more glass fragments falling off from the GF/PA6 pins which scratched the sliding surfaces, damaged the oxidative film and resulted in severe abrasion and adhesion in the fast cooled samples, hence leading to a high friction coefficient.

1. Introduction

The effects of composite microstructures on friction and wear have received much attention from tribologists in the last decade. Most studies have centred on the influences of reinforcement structures on friction coefficient and wear rate [1, 2], for example, filler size, orientation and fraction affect wear rates in sliding tests [3, 4].

The effects of microstructures of matrix and interface on friction and wear mechanisms have neglected to mention the area of tribological mechanisms relating to the transcrystallinity, crystallinity and phases of the matrix. Especially lacking are good tribologically and microstructurally based models for changes in the microstructure of these materials during moulding and applications. Thermal processing, an economical and effective method, can easily change microstructures and improve the properties of a thermoplastic composite. In particular, the cooling rate during moulding and annealing easily controlled in fabrication of industrial and commercial applications, has not been investigated in detail.

Understanding the relationships between thermal processing, microstructures, mechanical and tribological properties is essential for manufacturing thermoplastic composite materials. Many mechanical properties of thermoplastic composites, such as hardness and tensile strength, are dependent upon the degree of crystallinity which in turn is dependent upon the thermal history. Improving the mechanical and thermal properties of the thermoplastic composite materials can directly improve the wear resistance of the composites and enhance the limit of pv (loading pressure and velocity condition in tribological applications) values of the polymer composite materials.

The main objectives of this study are to provide a better fundamental understanding of the friction and wear mechanisms of thermoplastic composite materials as affected by processing methods and related material microstructure, and hence to find an optimized or tailored material microstructure that has a high wear resistance and a low friction coefficient.

A large number of experimental investigations were conducted in this paper to study the multiple wear and

friction mechanisms in pin-on-disk tests. Bulk GF/PA6 composite samples were selected to determine the relationship between the tribological mechanisms and material microstructures by controlling their cooling rates during thermal moulding. A theoretical friction model was established by an enormous theoretical analysis. Based on study the pv factor of the GF/PA6 with different moulding process, an empirical wear model was generated. To examine the damaging mechanisms of friction and wear, SEM (Scanning Electron Microscope), EDAX (Energy Dispersive Analytical X-ray) and XRD (X-ray diffraction examination) techniques were used.

2. Specimen preparation

Unidirectional GF/PA6 commingled yarn with a E-glass fibre weight fraction of 60% ($V_f = 40\%$) was supplied by Toyobo Co., Japan. The consolidating process of the composites was carried out at 240°C for 10 minutes with 1.5 MPa pressure by using a hydraulic hot-press machine. To obtain the different microstructures in the composites, three different cooling processes were conducted under 1.5 MPa pressure, cooled in cold water circling: −60°C/min, air circling: −3°C/min and cooled with hot- press: −1°C/min as Fig. 1 shows. The final dimensions of the GF/PA6 samples were 200 mm × 200 mm × 4 mm.

The specimens for the wear tests were cut from the GF/PA6 unidirectional bulk composite samples by using an electrical band saw at a speed of 550 m/min. To prevent the heat generated from the cutting damages the microstructure of the GF/PA6 samples, an air cooling was inducted. The specimens were cut to a size of 15 mm × 5.0 mm × 4.0 mm in three different directions which were parallel, transverse and normal to the unidirectional fibre orientation. The specimen was then inserted into a small steel tube, 8 mm in diameter and 10 mm in length, and mounted with epoxy adhesive (part A: 91% w/w liquid epoxy resin; part B: 100% w/w polyamide). Ten specimens for each cooling condition were prepared. Each specimen was polished with P600 emery paper which was stuck on the testing disk with double sided sticky tape. This procedure was carried out to obtain equal initial conditions e.g., same roughness of the pin surface and steel disk, for the wear tests.

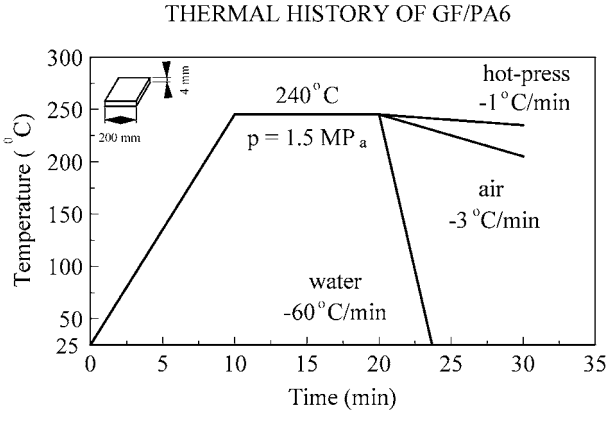

Figure 1 Thermal histories of GF/PA6 composite samples.

3. Experimental technique

3.1. X-ray diffraction examination

XRD tests were carried out on a Diffraktometer Siemens D5000 system to calculate the relative amounts of crystalline and amorphous material in a sample. The samples were 50 mm in diameter and 4 mm in thickness and were cut from the bulk GF/PA6 composites. The estimation of the amount of crystallinity is usually based on a comparison of the areas under the peaks (see Fig. 3). With proper attention to experimental detail, this method provides a reliable measure of crystallinity in polymers [5, 6]. 1 mm divergence slits and anti-scatter slits, a 0.2 mm receiving slit and a 0.6 mm detector slit were selected in this study. In this test, the speed of the detector scanning step was 0.040°/30s, low-angle X-ray diffraction ($2\theta = 10$°C to 40°C) and 60 rpm rotation were utilised. The samples were scanned for 6 hours 16 minutes and 30 seconds.

Worn debris were also examined by the X-ray Diffraction technique at room temperature to analyse the microstructure changes of the GF/PA6 in the wear tests. In this XRD examination, the speed of the detector scanning step was 0.040°/20 s and the angle of X-ray diffraction scanning, 2θ, was from 5° to 80° with continuous scan time of 10 hours and 25 minutes. The worn debris powder sample was fixed on to a holder without rotating operation. The 0.6 mm divergence slits and anti-scatter slit, 0.2 mm receiving slit and 0.6 mm detector slit were selected.

3.2. Pin-on-disk apparatus

Dry sliding tests were carried out on a commercial Plint wear and friction machine at room temperature to simulate steel components sliding over polymer composite bearing components. Fig. 2 shows a schematic view of the pin-on-disk apparatus. The specimens were laterally set against both sides of the spinning steel disk. The diameter of the sliding track was fixed at 80 mm on the steel disk. The speed of the steel disk can vary from 25 rpm to 2150 rpm (which is equivalent to a tangential velocity of 0.10 m/s to 9 m/s), by changing the gears. A load was applied to the end of the pins by two hydraulic cylinders which were easily adjusted by hydraulic pressure. The steel disk was made of AISI 4140 steel and the hardness of the disk is $H_v = 2450$ MPa. The surface of the disk was polished to a roughness of

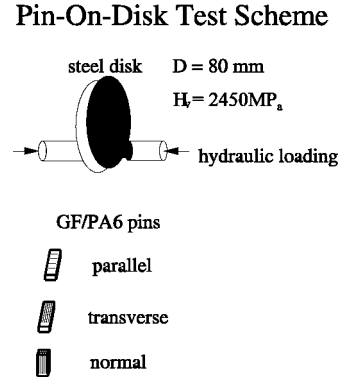

Figure 2 Schematic view of pin-on-disk test apparatus.

0.045–0.05 μm with P1200 emery paper and cleaned with methylated spirits prior to each test. The sliding directions were set up for parallel, transverse and normal to the fibre orientation.

The tangential force was measured by means of a pressure capsule attached to a slide carrying the two specimen pins. They were readily separated from the end loading forces, permitting particularly accurate measurements of friction coefficient. The signal from the transducer was taken to a force metre in the control cabinet and was recorded as one trace on the chart recorder. The sliding friction coefficient was calculated as

$$\mu = F/N$$

where $F =$ average value of friction force from both side pins (Newton) and $N =$ normal load applied on the end of the pin, by hydraulic cylinder (Newton).

With this system the wear depth was measured by the displacement transducers which were on either side of the cylinders. The signal from the transducer was taken to a displacement metre in the control cabinet and was recorded as another trace on the chart. The wear rate of the specimens were calculated by the following equation:

$$\text{Depth wear rate} \qquad w_t = \Delta h/t$$

where $\Delta h =$ wear depth (μm) and $t =$ sliding time (hour).

3.3. Microscopic study

The worn surface, subsurface and worn debris were examined by using a Philips 505 Scanning Electron Microscope. The specimens were sputter coated with a thin layer of carbon in order to improve the resolution of the specimen prior to the SEM examinations. For the low resolution of GF/PA6, an accelerating voltage was selected at 20 kV and the condenser lens (spot size) selected was 100 nm, both backscatter and secondary electron detectors were used.

3.4. Energy dispersive analytical X-ray study

An Energy Dispersive Analytical X-ray technique was used to analyse the contents of the elements in the worn debris. The X-ray microanalysis was carried out on a Philips 505 Scanning Electron Microscope with the life count time, 120 seconds for all the specimens.

4. Materials microstructure

Because the PA6 is a semicrystalline polymer, the crystal structures and amount of crystallinity of the polymer are often affected by thermal parameters during its fabrication. Further more, the mechanical or tribological properties of the GF/PA6 composite will be influenced by the amount and size of the spherulites of the PA6 [7]. These properties are also affected by the orientation of the spherulites which in terms of crystal phases. This phase terminology characterises the general conformation of the polyamide PA6 chains and their mode of packing, which results from thermal processing [8]. In other words, the crystal phases are determined by the intermolecular hydrogen bonding and chain packing in the spherulite crystals. In nylons, the spherulite crystals are formed from hydrogen-bonded sheets [9]. The crystal structures generally occur in one of four different phases: α, β, γ, or δ.

The α and γ phases normally coexist in bulk materials. The principal differences between these two phases are the lattice parameters and the orientation of the hydrogen bonds between the NH and the C=O groups. In the α phase, the hydrogen bonds are formed in the zigzag planes and between the antiparallel chains. The hydrogen bonded molecules are stacked upon one another forming planar sheets. The molecules are in the fully extended zigzag formation and theoretically can form strain-free intermolecular hydrogen bonds [9, 10]. In the γ phase, the molecular chains twist away from the zigzag planes to form hydrogen bonds between parallel chains. This twisting of the molecules results in a slight shortening of the periodicity in the chain direction, and results in the chain repeat distance of the γ form being shorter than for the α phase [11–13].

Our XRD results of the GF/PA6 composites showed that the microstructures of the composites were dramatically affected by changing cooling rate during thermal processes. Slow cooling resulted in a high crystallinity and formed more α phase than the fast cooling process. The lamellae thickness was slightly affected by the cooling rate as well.

In Fig. 3 [14, 15], it can be seen that there are two peaks appearing in all of the three cooling rate samples. The Bragg's angle θ of the first peak, which is from the right hand side, is over 23 degrees. The second peak is around 20 degrees. The two peaks represent the α and γ phases in the crystal structures of the PA6 matrix. Also it can been seen that there is a large proportion of amorphous phases in the background.

The area under the peaks present the crystalline volume of the polymer materials [5, 6]. The total peaks area, α plus γ, implies the proportion to the total volume of the crystalline PA6. The proportion of the peak areas of the three cooling rates samples was CI : CII : CIII $= 1 : 0.56 : 0.46$. Table I lists the proportional relationship between peak area and the crystallinity (X_c) of the PA6 matrix in the GF/PA6 composites. The Table I also lists the different ratios of the α and γ phases in the PA6 matrix due to the three different cooling processes.

From Table I, it also can be seen that the crystallinity of the air cooled samples (CII: X_c) was 20% which is quite close to the water cooled samples (CIII: X_c) 17%. This may probably be attributed to the crystalline forming speed of the PA6 was very fast. A previous study showed that it only takes 5 seconds for PA6 to achieve half its potential crystallinity at the fastest crystalline temperature 140°C. When the cooling rates are faster than −3°C/min, the different cooling rates would not make much difference to the crystallinity in the samples.

TABLE I The crystallinity of the GF/PA6 composites and peak area of the intensity in the XRD tests

Samples' cooling rate	$(\alpha+\gamma)$ peak area	Ration of α/γ	X_c of PA6
CI: -1°C/min (hot-press)	$127+4.72=131.72$	27	37%
CII: -3°C/min (air)	$52.94+20.62=73.56$	2.6	20%
CIII: -60°C/min (water)	$33.61+27.19=60.8$	1.2	17%

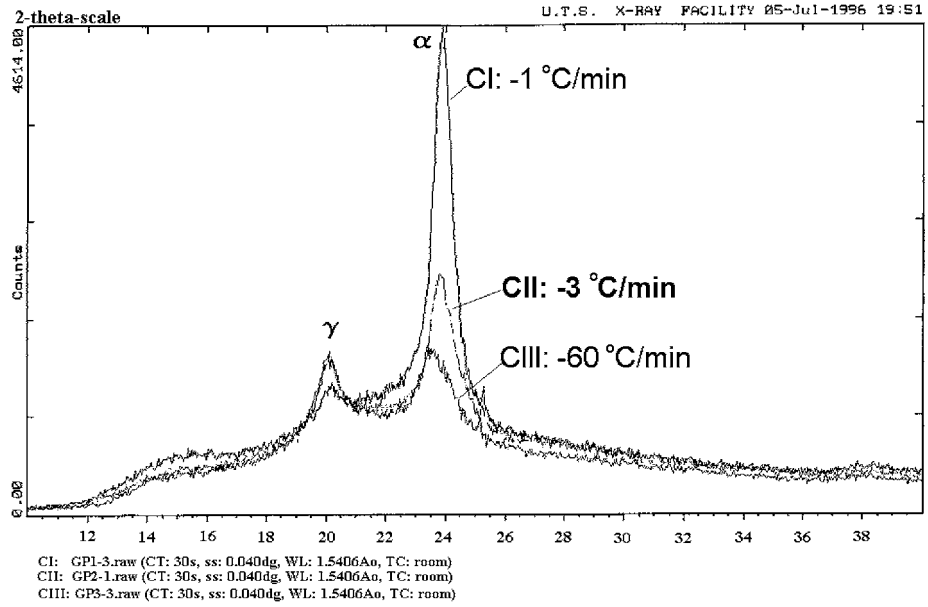

Figure 3 XRD diagram of GF/PA6 subjected to three different cooling rates.

In general, an amorphous polymer has a random distribution of chains in its main molecular structure. The structure gives rise to the viscoelastic nature of the PA6. A crystalline polymer shows considerable three-dimensional order. The different ways of molecular packing give a different density to the materials. The loosely packed amorphous materials have lower density than orderly packed crystalline materials. Thus to damage these orderly packed crystalline materials, more energy is required than for damaging the loosely packed amorphous materials. In fact, there are dramatic differences in such properties as elasticity, plasticity, hardness [10, 16] and thermal stability.

Therefore, the differences are not only in mechanical responses but also in tribological response when comparing the crystalline phases with the amorphous phases. When the working temperature reaches T_g (for the PA6 it is about 50°C), the amorphous polymer will become soft first and the crystalline phases may retain their properties until the temperature has reached its melting point.

As Fig. 3 and the Table I results show that the content of the α phase shift from high to low with the cooling rate increases but the γ phases have the trend opposite. Decreasing the cooling rate during moulding led to more α crystal structures formed than γ phase in the PA6 matrix. The CI samples have extremely higher contents of the α phase compared with CII and CIII samples. It also can be seen from Fig. 3, that CII and CIII samples have a similar volume of the γ phase to each other. The content of the γ phase in CI sample is less than that of CII and CIII samples.

A DSC test was conducted (and results were reported in a separate paper [14, 15]) to identify the melting point of α and γ phases of the GF/PA6 samples. It was found that the melting point of the α phase was higher than that of the γ phase. The high melting point of the α phase crystal structures in the GF/PA6 matrix will result in the composites samples having a higher service temperature than that of the γ phase and amorphous samples which were formed in faster cooling processes.

It has been reported that the hydrogen bonding angle of the α crystal is larger than that of γ crystal, thus the α chain is straighter and longer than that of the γ chain. The distance between adjacent chains in α crystal is shorter than that of the γ phase, thus the chains are packed tighter in α crystal than the γ crystal [12, 17]. Therefore, the density of α crystalline materials is higher than that of γ materials. Consequently, the hardness and Youngs modulus of α phase may be higher than that of γ phase.

There is some interesting evidence from Murthy and Bray's recent research [8] verifying the above assumption. PA6 specimens with a higher content of the α phase have higher density (1.24 g/cm^3), crystalline perfection, tensile strength and modulus than that of γ phase (1.17 g/cm^3). Their infrared spectroscopy and X-ray diffraction studies showed that to separate the γ phase and the amorphous scattering is very difficult when the γ phase is either poorly formed and/or is very low. The IR spectra of the γ phase and the amorphous are very similar to each other and very different from that of the α phase. This is because the γ chain and the amorphous chain possess very similar conformations. Murthy also

TABLE II XRD test results of the lamellar thickness of α crystallite in the PA6 matrix of GF/PA6 composites subjected to three different cooling rates

Cooling condition	2θ	β_m Measured FWHM	α Lamellar thickness
CI: -1°C/min hotpress cooled	23.891	1.0281°	79.36Å
CII: -3°C/min air cooled	23.864	1.1322°	71.99Å
CIII: -60°C/min water cooled	23.440	1.3346°	60.96Å

found that T_g increased with increasing proportions of α phase. Increasing T_g can result in low-wear materials in tribological applications [18].

The α phase has a higher thermodynamically stable structure than the γ phase. The heat of fusion of α phase (241 J/g) was found to be higher than the γ phase (239 J/g) [19]. The peak in mechanical loss (tangent δ) decreases with an increasing α phase crystallinity [20]. These characteristics of the α phase may give the composites a higher service temperature than that of the γ phase.

The XRD results also indicated that the full width at the half peak maximum intensity (FWHM) of the α phase in the three different cooling processed samples are CI: 1.028°, CII: 1.132°, CIII: 1.335°, respectively. This means the lamellar thickness was affected by the cooling rate as well.

Table II lists the thickness of the α phase lamellar crystal in the GF/PA6 matrix which were subjected to the three different cooling processes. The results showed that cooling rate has slightly affected the lamellar thickness. Slow cooling gave the PA6 thicker lamellar crystal than that of fast cooling process.

The thickness of lamellae can affect the mechanical properties of polymers. Increasing lamellar thickness (spherulite size) will result in decreasing toughness and rupture elongation, and increasing tensile strength and modulus of the polymers [21].

A polarised optical microscopy study [14, 15] of the GF/PA6 thin films showed that columnar spherulites grew along the glass fibres which may be transcrystalline layers. The columnar spherulites disappeared with increasing cooling rate. Different thickness of the transcrystalline layers were found to be influenced by the different cooling rate. Slow cooling led to a larger diameter of the columnar spherulites than the fast cooling process. The polarised optical microscopy results also showed that slow cooling led to larger size spherulites in the PA6 matrix than the fast cooling process.

The purpose of determining the various microstructural parameters described here is to attempt to predict the properties and performance of the GF/PA6 composites in its fabricating stage or during thermal processes. One of the most obvious differences that stands out in examining the X-ray scans of any sample was the relative amounts of the α and γ crystallinities. This α/γ ratio was quite useful because it reflected the manufacturing history of the GF/PA6 composites. The parameters that are likely to be directly useful in predicting the properties are the total crystallinity and the orientation of the matrix. The α and γ contents have significant influence on the mechanical and interfacial of the composites which were presented separately in other papers [14, 15]. In this paper the effect of these microstructural parameters of the materials on tribological properties will be discussed.

5. Friction mechanisms

In general, three stages of wear occurred during the continuous sliding test, running in wear, steady wear and severe wear. However, to investigate the cooling rate and microstructures of the samples influencing on the wear and friction mechanisms, only steady wear and friction mechanisms will be discussed in this paper.

By observing the worn surfaces of the GF/PA6 pins with the electron microscope, it was found that the damage mechanisms of the friction were very complex. Figs 4–6 are the SEM photos of the worn surfaces of

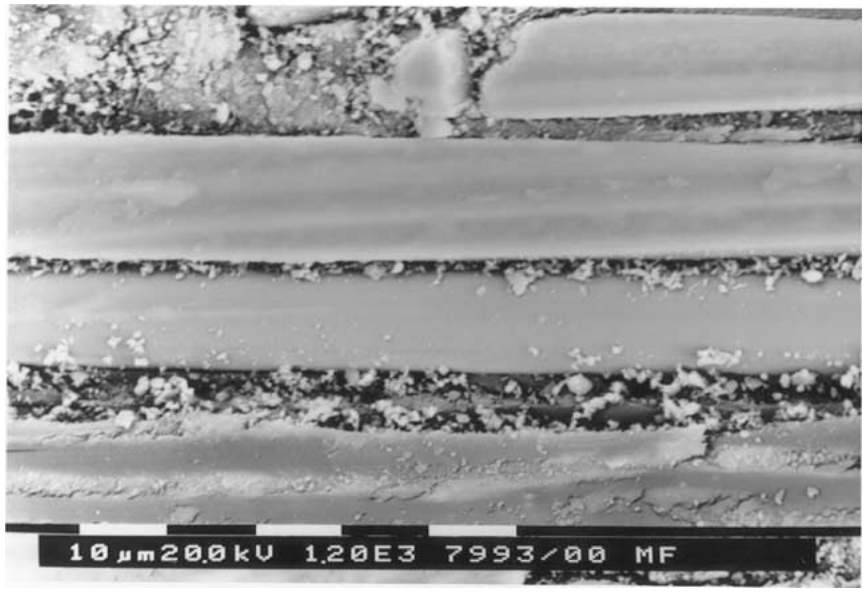

Figure 4 Worn surface of water cooled GF/PA6 pin after 20,000 metres sliding in parallel direction.

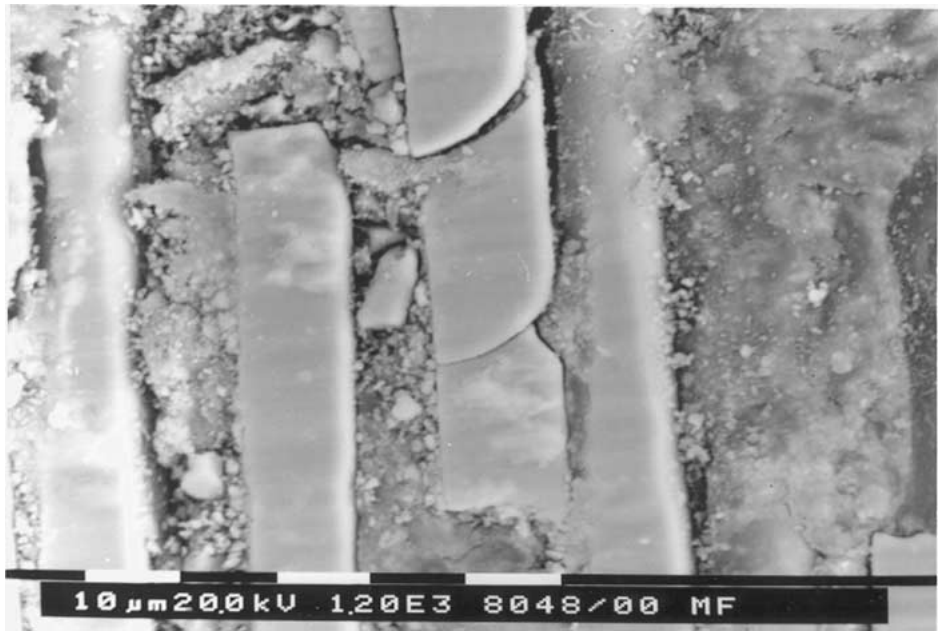

Figure 5 Worn surface of hot-press cooled GF/PA6 pin after 20,000 metres sliding in transverse direction.

Figure 6 Worn surface hot-press cooled of GF/PA6 pin after 20,000 metres sliding in normal direction.

the GF/PA6 composite pins slid in the parallel, transverse and normal directions, respectively. The photos were taken after the pin-on-disk tests with the loading pressure of 2.21 MPa, tangential velocity of 1 m/s and sliding distance of 20000 metres. It can be seen in the photos that the main mechanisms of the friction in the pin-on-disk test were fibre fracturing, interface debonding, matrix cracking and flaking. These phenomena occurred with all of the samples in the three sliding directions.

According to the SEM observation, the friction force of the present composite in the unlubricated pin-on-disk test, can be expressed as the sum of the following four components adhesion force in the PA6 matrix, plowing force, interfacial debonding and fibre fracture force.

$$F = F_a + F_p + F_i + F_f$$

In the tribological study of the GF/PA6 composite materials, the term of F_a was dependent upon the shear strength of the matrix which was in turn was dependent upon the cooling condition in the moulding processes. A slow cooling condition gave the matrix a higher crystallinity of the α phase in the PA6 which resulted in a higher density and greater shear strength material than that of fast cooling process.

The plowing term F_p was more complex in the pin-on-disk test than that of the single scratching test [22]. The plowing term was dependent upon the amount of the hard asperities and the roughness of the hard counterpart surface, the steel disk. In this case, the hard asperities consisted of glass fibre fragments and steel particles. They were all dependent upon the interfacial bonding conditions of the GF/PA6 composites which were controlled by the cooling conditions. The weaker

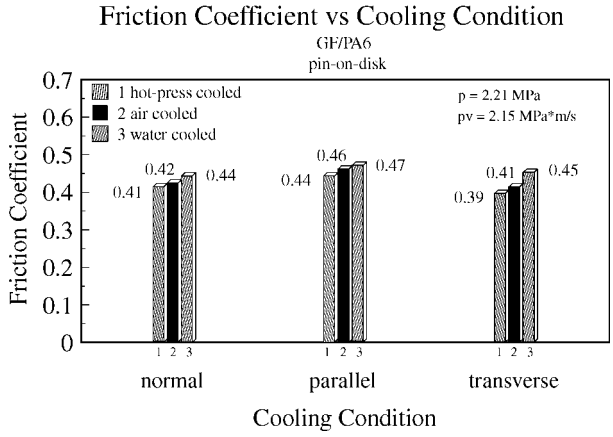

Figure 7 Friction coefficient of GF/PA6 versus cooling condition in three sliding directions.

the interfacial bond the more glass fibre fragments were breaking off from the matrix during the sliding test. The glass fibre fragments were then involved in the sliding surfaces and became hard particles plowing the composite pins and the steel disk surfaces. The plowing resulted in a rough surface of the steel disk. Then the rough steel disk and the particles plowed the surface of the composite pins.

The term F_i was dependent upon the strength of the interfacial bond between the glass fibres and the PA6 matrix which was influenced by the cooling condition. A slow cooling condition resulted in a higher transcrystallinity or stronger interfacial bond. The term F_f was dependent upon the strength of the fibre which was a constant for the E-glass fibre in these composite samples.

Fig. 7 shows the mean values of friction coefficient of the GF/PA6 composites in the parallel, transverse and normal directions with different cooling conditions in the moulding processes. The friction coefficient for each cooling condition pins tested were almost constant so that the standard deviation of the mean values was too small to be considered. The results indicated that the fast cooling gave a slightly higher value of friction coefficient at all fibre orientations/sliding directions. The friction coefficient of the hot-press cooled GF/PA6 pins (CI) was 6.4%, 7% and 14% less than that of the water cooled pins (CIII) in the parallel, normal and transverse directions, respectively. The differences of the three friction coefficient values are not that remarkable but the trend of the cooling rate influences on the friction coefficient can not be ignored either. There is a significant differences between the three cooling rates samples in wear and friction properties.

In the same sliding direction but with a different cooling condition, the friction caused by the adhesion, plowing and interfacial debonding terms were different due to the different crystallinity of the α phase and the interfacial strength. In the fast cooling condition, the reduced crystallinity of the α phase resulted in a low shear strength in the PA6 matrix. Thus, the adhesion term decreased while the cooling rate increased. Furthermore, fast cooling gave the composite a weak interfacial bonding condition which resulted in a decrease in the interfacial debonding term. The trend of the F_a and F_i was similar to that of the single scratch test. However, the situation was different in the plowing term. They were contrary to the trend of the scratching test results which have been presented in a separate paper by the same authors [22].

In the single scratching test, the fast cooling resulted in a softer matrix and weaker interfacial bond than that of the slow cooled samples. To plow the soft matrix and the weak interfacial bonded composite, the force was less than the plowing of the slow cooled composite samples. Thus, the term of F_p decreased with increasing cooling rate in the scratch test. The F_p term was only dependent upon the matrix hardness and the interfacial bonding condition since the hard particle was the diamond indenter which was a constant in the single scratch tests. Thus, the sum of the adhesive, plowing and interfacial debonding forces decreased with increasing the cooling rate.

In contrast to the scratching test, the F_p was not only dependent upon the hardness of matrix and the interfacial bond of the composites in the pin-on-disk test, but it was also dependent upon the amount of the hard particles, glass fibre fragments and steel debris. The fragments of the glass fibres were incorporated into the sliding surfaces as hard particles, and plowed the composite and the steel disk surfaces so that they formed asperities on the steel disk surface. The asperities of the steel disk surface plowed the composite pin surface and produced more glass fragments. The glass fibre fragments also scratched and damaged PA6 oxidative films between the sliding surfaces which may have been formed in the dry sliding process, to lubricate the sliding surfaces and reduce the friction. Weak interfacial bonding conditions led to a large amount of the glass fibres debonding from the composite pins and this increased the plowing term in the sliding test.

An Energy Dispersive Analytical X-ray (EDAX) study of the worn debris verified the above analysis. Fig. 8 shows a typical energy dispersive spectra of the worn debris of the GF/PA6 pin after 20000 metres of sliding against the steel disk in the transverse direction. The contents of the Si and Ca were found to be greater in the debris of the fast cooled samples than that of the slow cooled samples as Table III shows. The Table III shows the x-ray photon counts of Si and Ca elements in the three types worn debris from the three different cooling conditions samples GF/PA6 pins transversely sliding on the steel disk.

The Si and Ca are the main compositions of the E-glass fibres. Thus, it can be concluded that there

TABLE III X-ray photon counts of Si and Ca elements in energy dispersive spectra from EDAX test results of worn debris of GF/PA6 and steel disk

Cooling condition of GF/PA6 samples	x-ray photon counts of Si in energy dispersive spectra	x-ray photon counts of Ca in energy dispersive spectra
Hot-press cooling	6420	1780
Air cooling	6740	1870
Water cooling	7210	2100

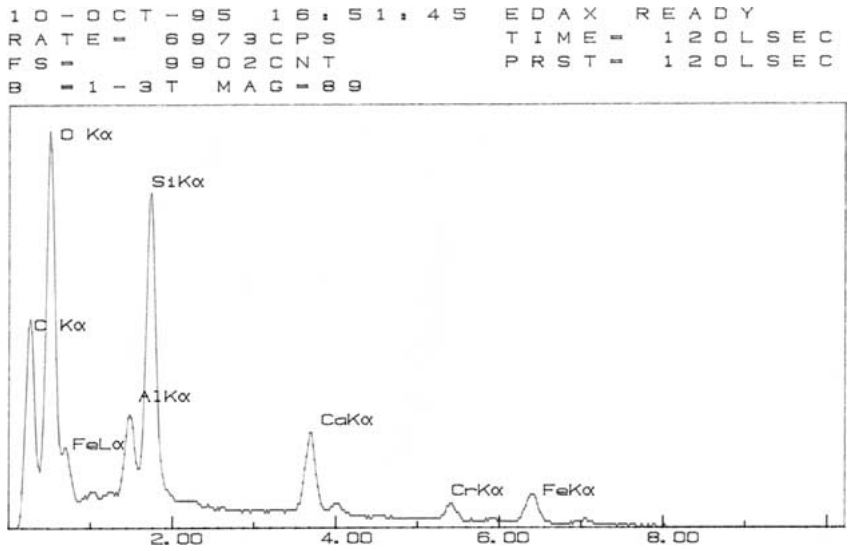

Figure 8 Energy dispersive spectrum of worn debris of GF/PA6 pin cooled in hot-press and transversely sliding over steel disk for 20,000 metres distance with $p = 2.21$ MPa and $v = 1$ m/s (Y axis: Total x-ray photon counts, X axis: x-ray photon energy, KeV).

were more glass fibre fragments in the worn debris of the fast cooled sample than that of the slow cooled samples.

It was also found that the Fe and Cr contents were greater in the worn debris of the fast cooled samples than that of the slow cooled samples from the EDAX results. The Fe and Cr elements are the main compositions of the 4140 steel disk. This means the steel disk was severely ground off by the glass fibre fragments with the fast cooled sample pins than that of slow cooled sample pins. The surface roughness observation of the steel disk after the sliding test also verified the above analysis. The steel disk roughness was measured after sliding the same distance and under the same loading/speeding condition with the GF/PA6 pins subjected to the three different cooling conditions. The steel disk was rougher after sliding with the fast cooled GF/PA6 pins than that of slow cooled pins.

It is reasonable to conclude that the effect of the interfacial bonding condition on the plowing friction was more important than that of the matrix properties in the pin-on- disk test. The plowing term increased while decreasing the interfacial bonding strength which was caused by the fast cooling. The plowing term dominated the friction mechanisms in the pin-on-disk tests. The component of the plowing term was greater than the rest of the three components. Thus, the friction coefficient increased with increasing cooling rate.

6. Wear mechanisms and resistance

In general, wear mechanisms can be classified into four groups: Adhesive wear, Abrasive wear, Fatigue wear, Corrosive wear. However, in some of the wear stages and under certain circumstances, there are always one or two wear mechanisms dominating the wear processes. This depends upon the pair of counterpart materials and working conditions. For example, adhesive wear mechanism governs the steady wear stage in an unlubricated and clean metal surface [23]. On the other hand, abrasive wear is the main wear mechanism in a running-in stage when the sliding has just started with a hard and rough counterface on a soft bearing. What are the most important wear mechanisms in the steady wear stage of the fibre reinforced polymer composites? How do the microstructures and thermal histories of the composites affect these mechanisms?

In fact, it was found in this study that the dominant wear mechanisms of these materials in the pin-on-disk test during the steady wear stage were oxidizing, carbonising, abrasion, interfacial debonding and adhesion. They will be discussed in detail and separately in the sections below.

6.1. Oxidizing and carbonising wear

Generally PA6 becomes reddish brown in colour when it is heated to its molten state between the temperatures of 225°C–245°C and exposed to air. While this is occurring, the PA6 is thermally oxidised, degraded and depolymerized. The influence of the temperature and water on the depolymerization of the polymer has been studied by many material scientists [24, 25]. The oxidative degradation of the polyamides has been discussed in detail by Nobuya [26]. He indicated that the major products obtained from the pyrolysis of PA6 were water, carbon dioxide and carbon monoxide. It was also found that the amorphous region was more likely to be attacked by heat than the crystalline region [27].

In this study, similar phenomena were found in the thermal moulding processes of the GF/PA6 composite and in the pin-on-disk wear test. During the thermal moulding processes of the GF/PA6 composite, some of the PA6 oozed out from the gap at the side of the mould and exposed to the air become a reddish brown in colour. However, the inside part of the sample was white in colour due to it being sealed inside the mould where it was protected from the air.

During the wear test, the friction heat was trapped in the sliding surfaces and formed some very hot spots on the composite pin surface. This heat may cause the surface to melt or soften. The thermal conductivities and melting point of the polymers are very low. Therefore, oxidizing and/or carbonising wear may occur in the

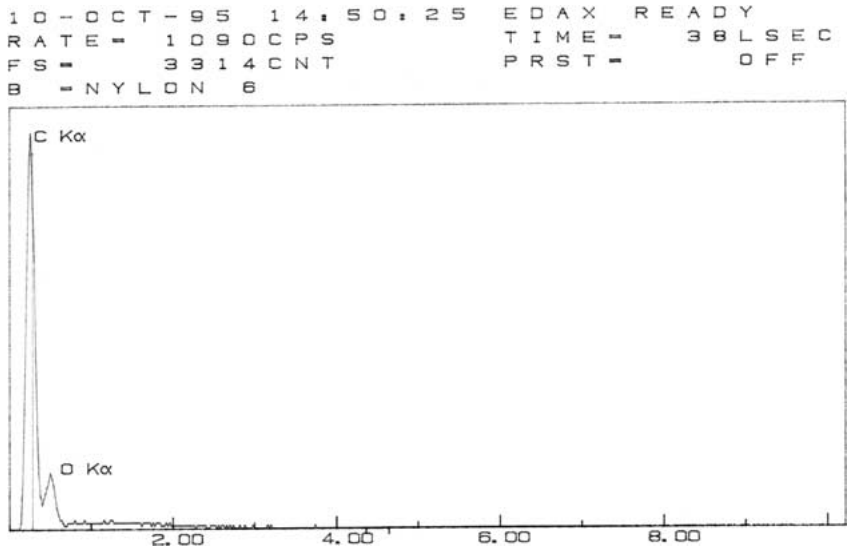

Figure 9 Energy dispersive spectra of PA6 before wear test (Y axis: Total x-ray photon counts, X axis: x-ray photon energy, KeV).

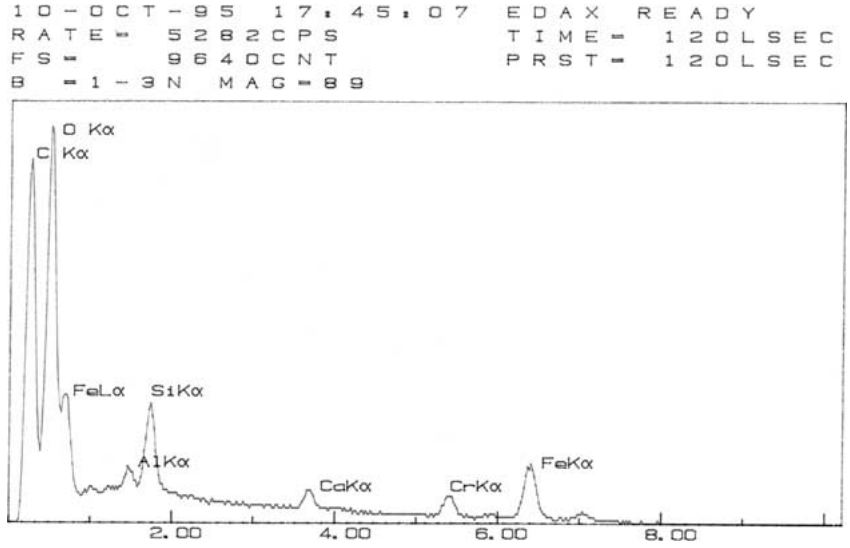

Figure 10 Energy dispersive spectrum of worn debris of GF/PA6 pin cooled in hot-press and normally sliding over steel disk for 20,000 metres distance with $p = 2.21$ MPa and $v = 1$ m/s (Y axis: Total x-ray photon counts, X axis: x-ray photon energy, KeV).

wear test. This was verified by observing the colour of the worn surface and the worn debris. The worn surface and debris became brown or black after the wear test. This was also verified by the EDAX results. Fig. 9 shows the PA6 spectrum before the wear tests while Fig. 10 shows the worn debris after the pin-on-disk wear test in the normal sliding direction with the speed/load condition of $v = 1$ m/s and $p = 2.21$ MPa. The EDAX results showed that the content of O and C elements were significantly higher in the worn debris than that of PA6 sample before the wear tests as Table IV shows. Table IV shows respectively the X-ray photon counts of the O and C elements in the worn debris were 28 times and 2.26 times higher than that of the PA6 sample before the wear test. The GF/PA6 composite pins were cooled in hot-press and sliding in normal direction against the steel disk.

Therefore, it can be concluded that the oxidative degradation and carbonising wear occurred during the wear tests. They may be the main wear mechanisms in the polymer composites.

TABLE IV X-ray photon counts of the O and C elements in the energy dispersive spectra from the EDAX test results of the PA6 sample before the wear test and the worn debris of the GF/PA6 and the steel disk after the wear test

EDAX test samples	x-ray photon counts of O in energy dispersive spectra	x-ray photon counts of C in energy dispersive spectra
PA6 before wear test	260	2920
GF/PA6 & steel worn debris	7380	6610

The oxidization can be useful in the wear application when the oxidative film formed. The effect of an oxidative film on polymer wear is similar to a metal oxidative film, reducing friction and lubricating the sliding surfaces. The oxidative film can prevent the contact between the pin surface and the steel disk surface, and effectively reduce the adhesive wear [28]. However, the harmful side of the oxidizing may result in

depolymerization and decomposition in the polymer composites. As a consequence of the depolymerization and decomposition, the composite surface mechanical strength and hardness may be reduced and lead to severe wear.

When the contact surfaces getting too hot carbonisation occurs after the oxidization in the wear applications. Unlike the oxidization which can be useful in the wear, carbonising wear has always been detrimental under any circumstance in the polymer composites wear applications. Carbonisation can form hard particles which would be involved in the contact surfaces and increase abrasive wear.

Increasing the polymer thermal stability can reduce the occurrence of thermal degradation, oxidizing and carbonising in the wear application. Slow cooling can improve the thermal stability of the PA6 in the moulding process. Slow cooling gave a higher crystallinity and a higher content of α phase in the PA6 matrix than the fast cooling process. As mentioned in Section 4, the α phase has a higher thermodynamically stable structures and higher heat of fusion in its crystalline structures than that of the γ phase and the amorphous phase. The peak of the mechanical loss (tangent δ) at high temperature range (70°C–90°C) decreases with an increase of the α phase crystallinity [29]. These characters of the α phase give the slow cooled GF/PA6 composites a higher service temperature and higher abrasive wear resistance at the high temperature range than the γ phase and amorphous of the PA6.

It will be discussed in detail in the next few sections how the cooling rate affected the abrasive and adhesive wear mechanisms, and how the oxidizing wear, abrasive wear and adhesive wear interacted with each other during the pin-on-disk wear test.

6.2. Abrasive wear and interfacial debonding

According to the friction analysis of the unlubricated continuous sliding test in Section 5, it is not difficult to assume that a fast cooling process could result in a lower wear resistance in the GF/PA6 composite pins than the slow cooling process. The reason is that the fast cooling gives the material a softer matrix and weaker interfacial bond than the slow cooling. When the hard asperities of the steel disk were sliding on the composite surface, the fibres and matrix were abrasively worn off or plowed out. A softer matrix was easily plowed or cut by the asperities than the harder matrix. The fibres were easily debonded in the weak interfacial bond composite than strong interfacial bonding composite. The debonded or pulled out glass fibre fragments became hard particles cutting or grinding the steel disk surface producing more hard asperities on the surface of the steel disk. The glass fibre fragments and the asperities of the steel disk led to further abrasive wear and so on. The following results verified the above assumption.

In general, abrasive wear resistance is proportional to the hardness, shear strength, compressive elastic modulus and yield strength of the softer counterpart [30, 31]. In this study, it was discovered that the interfacial bond also played a very important role in the abrasive wear of the composites. As discussed in the Section 5, the SEM photos of the worn surfaces of the GF/PA6 composite pins after a sliding of 20000 metres distance with loading pressure of 2.21 MPa and tangential velocity of 1 m/s in the parallel, transverse and normal directions, respectively (see Figs 4–6), revealed that interface debonding occurred in all sliding directions. It also can be seen clearly in the SEM photos of the worn subsurface (see Figs 11 and 12) that the interface debonding did not only occur on the sliding surface but also occurred in the deep subsurface. The SEM photos were taken from the lateral view of the pin specimens after the wear tests. The interfacial debonding of the subsurface can be evidenced approximately 50 microns deep down from the worn surface. The EDAX evidence also proved that there were more glass fibre fragments pulled out from fast cooled pins than the slow cooled pins as mentioned in Section 5.

Glass fibres played a very important role in the wear applications. They can enhance thermal conductivity to release friction heat from the sliding surfaces and

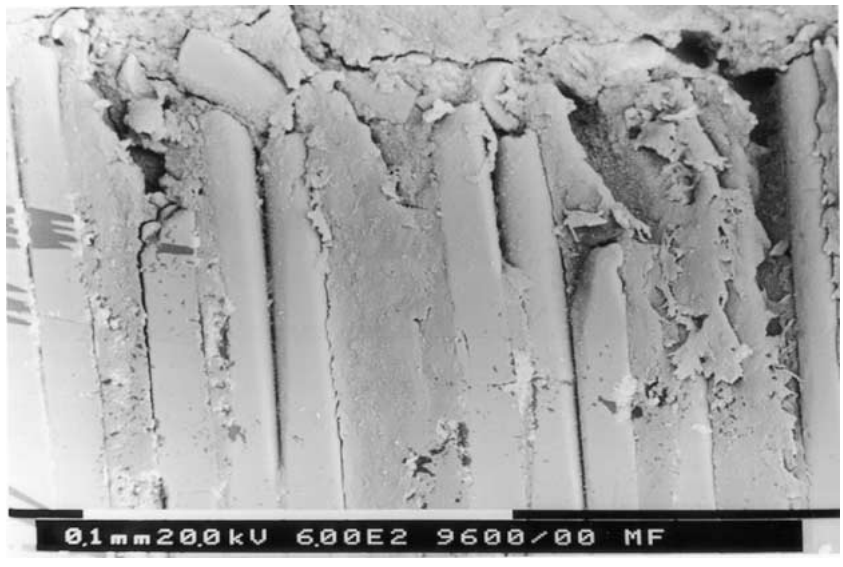

Figure 11 SEM photo of worn subsurface taken from the lateral view of the water cooled GF/PA6 specimen.

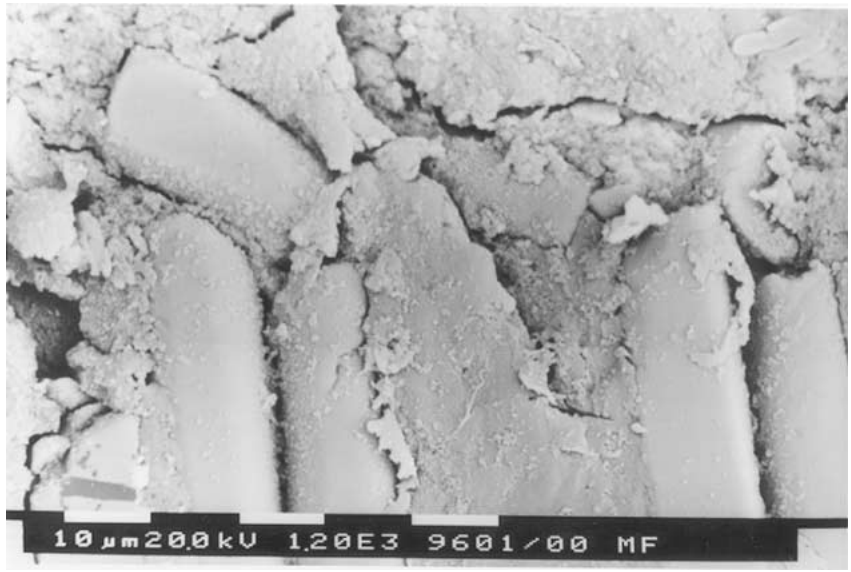

Figure 12 SEM photo of worn subsurface taken from the lateral view of the water cooled GF/PA6 specimen.

improve the strength and stiffness of the material. When the fibres were bonded in the matrix, they supported a majority of the normal load and reduced the steel asperity tips penetrating into the PA6 matrix. As a consequence of the glass fibre effects, the microcutting or microplowing mechanisms were not as effective. However, when the fibres were debonded and pulled out from the matrix, the fibres act as hard particles enhancing the abrasive wear on the pin surface. The PA6 matrix without the glass fibres reinforcing them would fail with compression and thermal decomposition, thus it would be worn quickly.

A pure cast raw PA6 pin was tested in the pin-on-disk wear machine with same loading and speeding condition of GF/PA6 pins, $p = 2.21$ MPa and $v = 1$ m/s. This test was conducted to compare the tribological characters of the pure PA6 polymer and the GF/PA6 composite. The PA6 pin was softened and molten by the friction heat after sliding distance of 943.5 metres at running-in stage. In a fact, the specific wear rate of the pure PA6 pin was 59.33×10^{-6} mm^3/N* m, and it was 5 times higher than the GF/PA6 pin with same load/speed condition. The friction coefficient of the PA6 pin was 0.74, and it was twice of the GF/PA6 pin. The PA6 pins finally failed with its surface melted and pin soften bent after 940 metres sliding distance in the running-in stage.

The wear rate test of the GF/PA6 composites were performed at a constant normal loading pressure and a constant sliding velocity. Figs 13 and 14 reveal the influence of the cooling rate on the specific wear rate of the GF/PA6 composites sliding in normal and transverse directions, respectively. With this configuration system the wear volume was calculated by wear depth times wear surface area which is the section area of the pin. The wear depth was measured by the displacement transducers which were on either side of the cylinders. The specific wear rate of the GF/PA6 specimens was then calculated by the following equation.

$$w_s = \Delta V/(N^* L)$$

where ΔV = wear volume (mm^3), N = normal load (Newton), and L = sliding length (m).

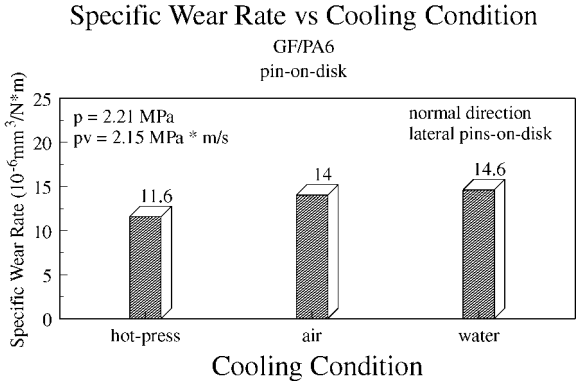

Figure 13 Specific wear rate of GF/PA6 pin versus cooling condition in normal sliding direction.

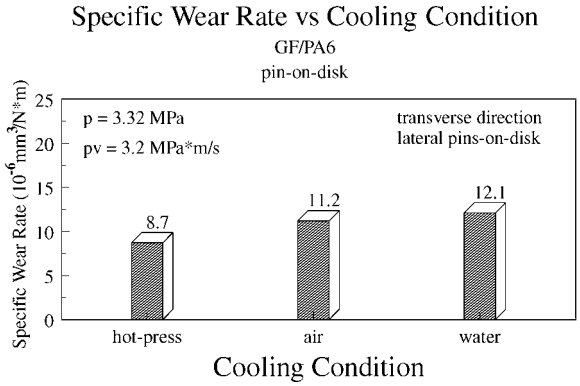

Figure 14 Specific wear rate of GF/PA6 pin versus cooling condition in transverse sliding direction.

Figs 13 and 14 show the trend of the wear rate varied with the cooling conditions. These values are mean values from each wear test. The slow cooling condition resulted in a low value of the specific wear rate in the two sliding directions when compared with the faster cooling conditions. The specific wear rate of the GF/PA6 pins cooled with hot-press was reduced 21% and 28% when compared with the water cooled pins in the normal and transverse directions, respectively. According to the above results, it can be inferred that the

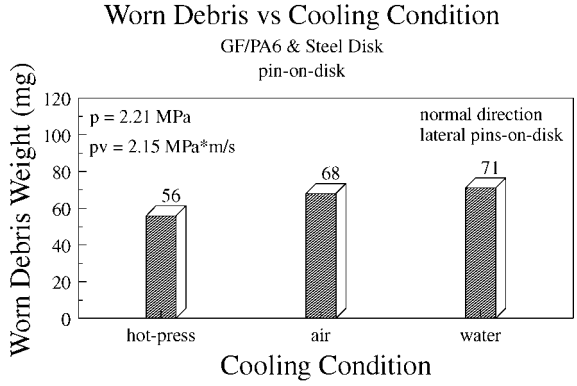

Figure 15 Worn debris weight of GF/PA6 pin normally sliding over steel disk for 20,000 metres distance wit $p = 2.21$ MPa and $v = 1$ m/s, versus cooling condition.

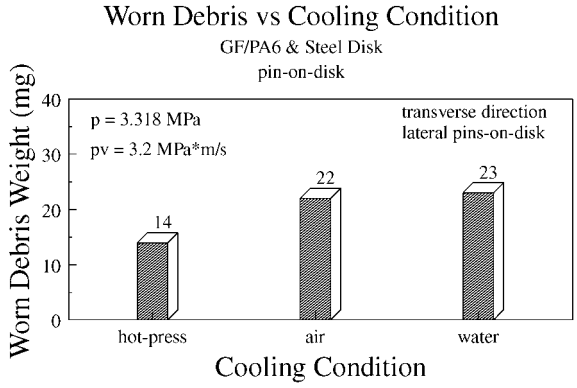

Figure 16 Worn debris weight of GF/PA6 pin transversely sliding over steel disk for 25,000 metres, distance with $p = 3.32$ MPa and $v = 1$ m/s, versus cooling condition.

wear resistance increases with decreasing cooling rate. Indeed these results can be further manifested by the weight measurement of the worn debris. Figs 15 and 16 show the effect of the cooling rate on the weight of worn debris in the normal and transverse sliding directions, respectively. The weight of the worn debris varied remarkably with the changes in the cooling condition. The worn debris weight of the cooled with hot-press GF/PA6 pin slid on the steel disk was 30% and 40% less when compared with the water cooled pin slid on the steel disk in the normal and transverse directions, respectively. The trend of the worn debris was similar to the specific wear rate measurement results. However, the difference of the worn debris and specific wear rate measurements was the specific wear rate measured the pure GF/PA6 volume lost, but the worn debris was the sum of the steel debris and the GF/PA6 debris. As it can be seen in the EDAX results, the fastest cooled pins sliding on the steel disk resulted in more Fe and Cr elements in the debris than that of slow cooled pins. This means the fast cooled sample ground more steel disk than the slow cooled one due to the debonded glass fibre fragments from the fast cooled pin. The fragments of the glass fibre caused the abrasive wear on the both side of sliding surfaces, the GF/PA6 pin and the steel disk. The roughness of the steel disk surface was measured after each test and it was found that the steel disk surface was rougher with the fast cooled sample sliding on the steel disk than that of slow cooled samples.

Apart from the interfacial bonding condition affecting the abrasive wear of the GF/PA6, the mechanical properties of the matrix, such as shear strength and hardness of the GF/PA6 composite also contributed to the abrasive wear. Since the slow cooling gives the GF/PA6 pins higher content of the α phase crystalline in the PA6 matrix than the fast cooling process did, the strength and hardness of the slow cooled pins are greater than the fast cooled pins. It needed more energy to plow or cut the α phase crystalline matrix than the γ phase and amorphous matrix by the hard particles or asperities in the pin-on-disk tests. As the cohesion of the α phase crystalline structure is stronger than that of the γ phase and amorphous, therefore, the slow cooling resulted in a lower abrasive wear than the fast cooling.

However, in the instance of high temperature, the mechanical properties of the thermoplastic composites may change. They can be affected by the friction heat generated during the wear tests. In a high temperature situation, the PA6 may be thermally oxidatively degraded and depolymerized or melted by the friction heat, and completely lose its mechanical properties. In other words the abrasive wear of the thermoplastic composites, in the continuous dry sliding tests, were dependent upon the mechanical properties and the thermal stabilities of the material. The thermal stabilities of the GF/PA6 were dependent upon the crystallinity of the α phase, the melting point and the glass transition temperature of the PA6 matrix. Due to the thermal conductivity of the polymers are very low, the friction heat can not dissipate quickly and the sliding surface temperature will rise. When the temperature reaches a certain point the polymer surface starts to melt or thermally decomposed and the material reaches its service limit. Therefore, improving the thermal stabilities of the polymer will lead to an increase of the service limit.

The GF/PA6 pins were detected by the XRD before the wear tests. As Fig. 3 shows there were two crystalline forms and an amorphous form existing in the PA6 matrix of the GF/PA6 composites. After the wear test, the worn debris was examined by the X- ray diffraction technique. Figs 17–19 show the XRD results of the worn debris. The X-ray diffraction results of the worn debris were completely different when compared with the XRD results of the GF/PA6 before the wear tests (see Fig. 3). The α and γ phases formed in the moulding process were completely destroyed by the friction heat in the debris. There could be at least two possibilities causing the former crystalline structures to disappear. The first possibility perhaps is that the temperature on the sliding surface reached the melting point of the PA6 and then the PA6 melted and then formed different structures. Another possibility may be the sliding surface temperature reached the annealing temperature of the PA6 which is 80°C. The debris fell off from the hot sliding surfaces and cooled down in the air and then quickly formed another structure and/or an amorphous material. The sliding surface temperature was measured by using an infrared thermometer. The results of the infrared measurement showed that the surface temperature only reached 85°C–110°C. It is therefore reasonable to assume that the structure changes in

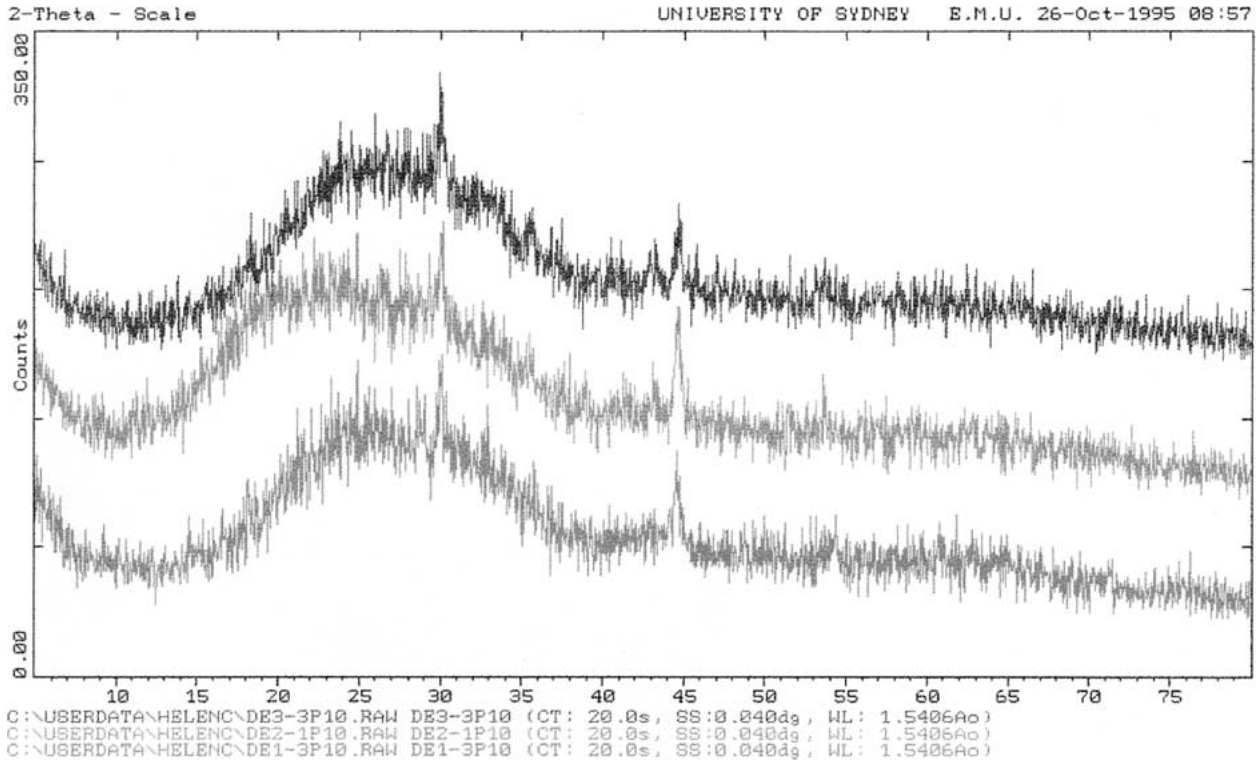

Figure 17 X-ray diffraction scattering curves of worn debris of GF/PA6 pin cooled in three different cooling conditions and parallel sliding over steel disk for 20,000 metres distance with $p = 2.21$ MPa and $v = 1$ m/s.

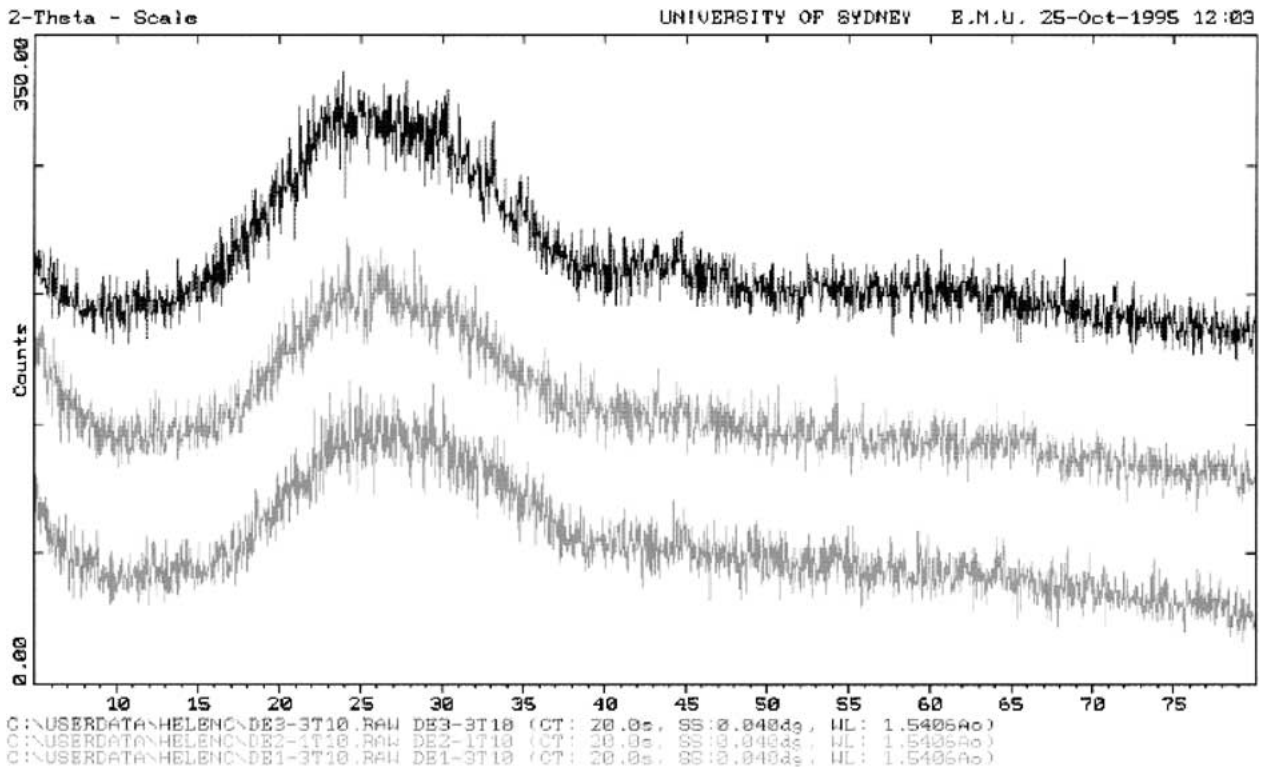

Figure 18 X-ray diffraction scattering curves of worn debris of GF/PA6 pin cooled in three different cooling conditions and transversely sliding over steel disk for 20,000 metres distance with $p = 2.21$ MPa and $v = 1$ m/s.

the worn debris were mainly due to the second possibility, annealing processes during the wear tests.

However, no matter which of these was the case, the XRD results of the worn debris showed that the friction heat has destroyed all of the crystalline structures which were formed during the fabricate moulding process. There was no original crystalline structure observed in the debris after the sliding test. Owing to the high cohesion of the α phase and the endothermic fusion of the α phase crystalline, to destroy the α phase crystalline needs more energy than that of γ phase. Due to a slow cooling condition the PA6 matrix was a higher crystallinity and greater amount of α phases than with fast cooling process, thus the abrasive wear resistance

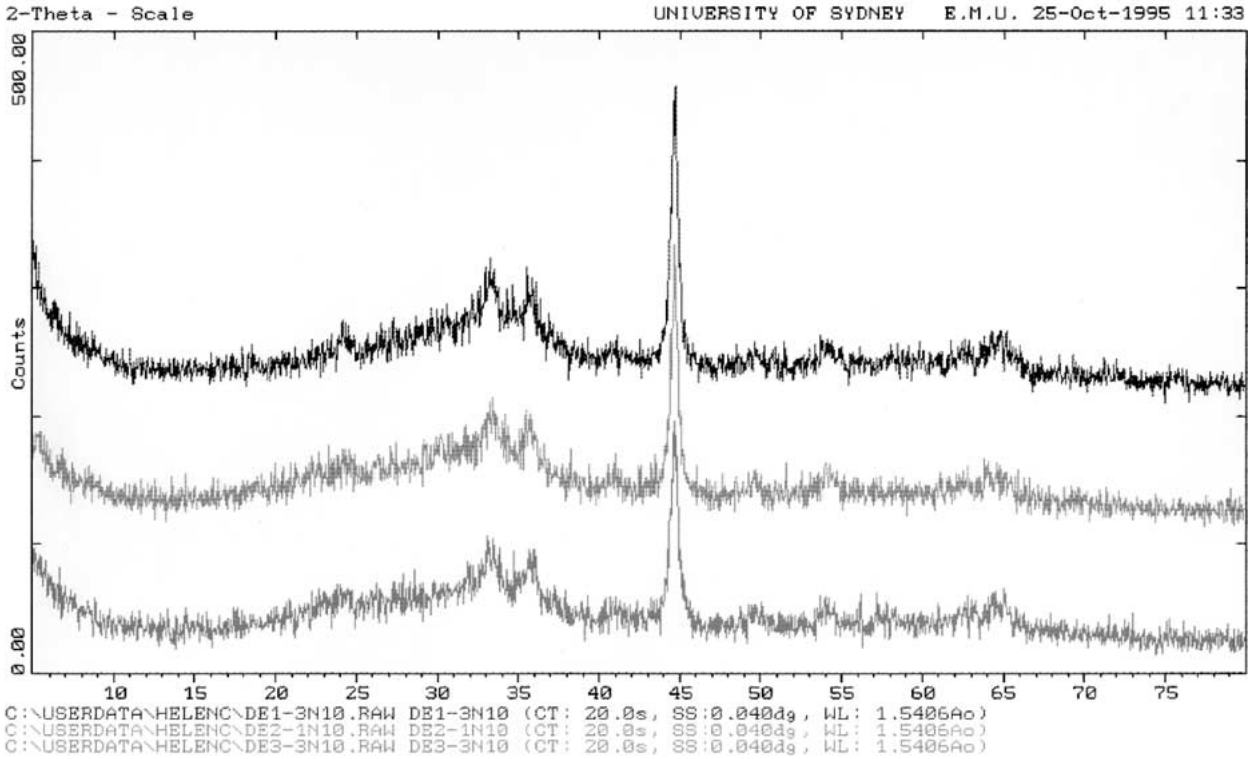

Figure 19 X-ray diffraction scattering curves of worn debris of GF/PA6 pin cooled in three different cooling conditions and normally sliding over steel disk for 20,000 metres distance with $p = 2.21$ MPa and $v = 1$ m/s.

was higher with the slow cooled GF/PA6 pins than that of fast cooled pins.

Moreover, when the temperature reached the glass transition point of the amorphous matrix during the sliding test, the amorphous matrix started to become soft and viscous. The soften amorphous matrix can't hold the glass fibres any longer, thus the fibres debonded and became hard particles involving into the sliding surfaces and increasing the abrasive wear. A slow cooling may result in a higher T_g in the amorphous PA6 matrix than the fast cooling process [32]. Increasing T_g can lead to an increase of wear resistance of the polymers [18]. Thus, the high T_g may contribute to the low abrasive wear of the slow cooled GF/PA6 composite pins as well.

6.3. Adhesive wear

Figs 20–22 show the SEM photos of the worn surfaces of the GF/PA6 pins which were subjected to the slow cooling process in the hot-press and then slid over the steel disk in the parallel, transverse and normal directions, respectively. The SEM photos show that flakes of the PA6 matrix accumulated on the worn surfaces of the

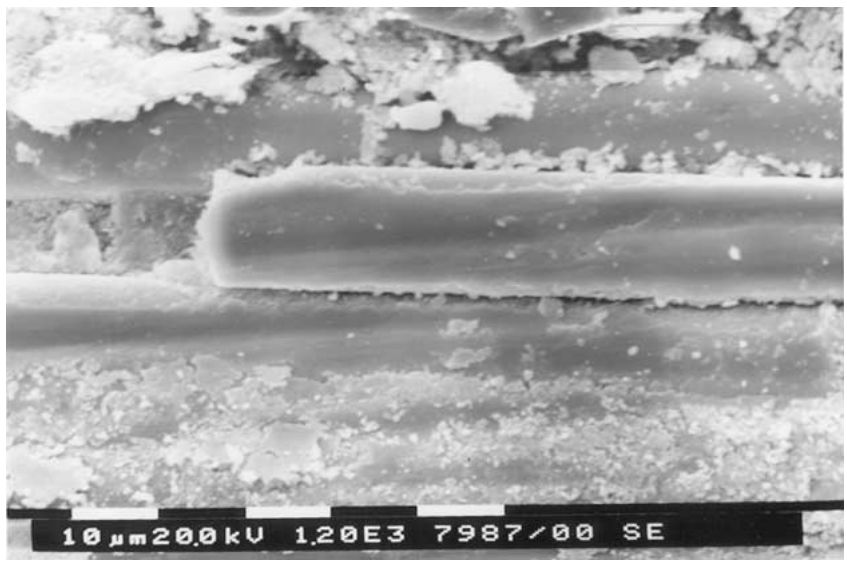

Figure 20 Worn surface of GF/PA6 pin cooled in hot-press after 20,000 metres sliding in parallel direction.

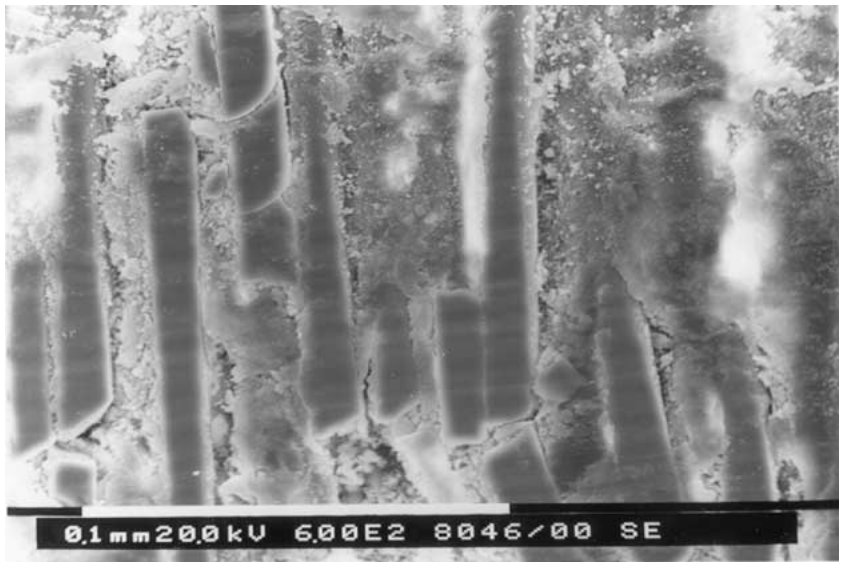

Figure 21 Worn surface of GF/PA6 pin cooled in hot-press after 20,000 metres sliding in transverse direction.

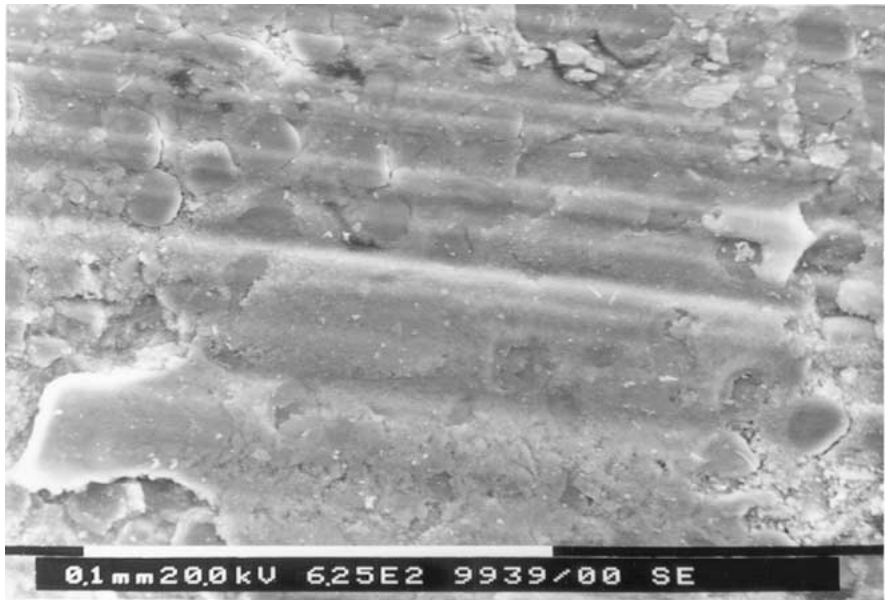

Figure 22 Worn surface of GF/PA6 pin cooled in hot-press after 20,000 metres sliding in normal direction.

pins. The optical microscopy observation also show that brown PA6 film was transferred on to the sliding surface of the steel disk. According to the above evidence, it can be suggested that the adhesive wear occurred on the sliding surfaces during the sliding tests.

The adhesive wear volume is inversely proportional to the shear strength, yield strength and hardness of the soft counterface [33]. The shear strength of the PA6 matrix was much lower than that of the steel disk and the shear strength of the glass fibre was higher than that of the steel disk, thus the adhesion or shear cutting normally occurred either in the subsurface of the matrix or on the surface of the steel disk. This depended on the glass fibre distribution. In the fibre concentrating area, the adhesion occurred on the steel disk surface or subsurface. In the matrix rich region the adhesion occurred in the subsurface or surface of the pin. The adhesion wear generally is caused by a cohesive failure of the material due to the shear stress exceeding the shear strength of the material. Since the slow cooling gives the GF/PA6 composite a stronger cohesion or a higher shear strength than that of fast cooling, the adhesive wear was less in the slow cooled GF/PA6 pins than that of fast cooled pins.

When an oxidative film formed between the sliding surfaces, the adhesion wear occurred in the film instead of in the matrix or the steel disk. The shear strength of the oxidative film was much lower than that of nylon matrix and steel disk as the film is a thermal oxidized product of the PA6, depolymerized polymer. Therefore, the adhesion or shear cutting almost occurred in the oxidative film. The film acted as a boundary lubrication in the sliding surfaces.

When the oxidative film was damaged by the asperities of the steel disk and/or glass fibre fragments, the adhesion occurred on the surface or in the subsurface of the composite pins and the steel disk. The mechanical properties of the matrix and the interfacial bonding

condition between matrix and fibres were very important in the adhesion wear. Low shear strength, soft matrix and weak interfacial bond would result in severe adhesive wear. However, since the slow cooling resulted in a harder matrix and stronger interfacial bond than that of fast cooling, again the adhesive wear of the slow cooled GF/PA6 pins was less than that of fast cooled pins.

7. Effect of mould cooling rate on *pv* factor and an empirical wear model

When one solid body is sliding over another the most of the work done against the frictional force opposing the motion will be liberated as heat between the surfaces. This heat will be carried away from the surfaces by conduction and radiation, but for polymer bearings due to their low thermal conductivity the surface temperatures may reach very high values. The surface temperature increases with an increase in the sliding velocity or normal load of the sliding body. In excess of loading pressure (p) and velocity (v) limits, the polymer bearing would fail rapidly due to melting or thermal decomposition. Improving the mechanical properties and thermal stability of the polymer composite bearing materials can directly enhance the limit of the pv values.

In this section the pin-on-disk tests were carried out with variable pv values to investigate the influence of cooling condition on wear rate and pv limit of the GF/PA6 composites.

The wear rate of a pure polymer bearing is obviously a function of load and speed (pv). As a bearing material will give the desired lifetime under a specified conditions of load and speed, the pv factor is a very important parameter in industrial bearing design. Based on the reasonable assumption that the wear rate is proportional to the rate of energy dissipation at the sliding surfaces, Halling derived a linear function between the depth wear rate and the pv for pure polymer bearing as following [34].

$$w_t = k_o pv$$

where the k_o is a constant wear factor. Under a critical pv condition, the k_o is equal to the specific wear rate, w_s.

However, for polymer composite bearing the relationship between the wear rate and pv is not that simple. Based on a large number of experimental data, a new empirical model was established by using the least square method in this study. The relationship between depth wear rate and pv factor can be described by an exponential regression line. Fig. 23 shows the depth wear rate of the GF/PA6 composite under different pv condition in the pin-on-disk tests The results revealed the relationship between the depth wear rate and pv factor of GF/PA6 composites with different cooling rate samples in the normal sliding direction. The results were regressed to a exponential curves with regressive root-square coefficient of 0.97, 0.91 and 0.96 for hot-press, air and water cooled samples, respectively. The exponential regression relationship for the specific composites, the GF/PA6, was

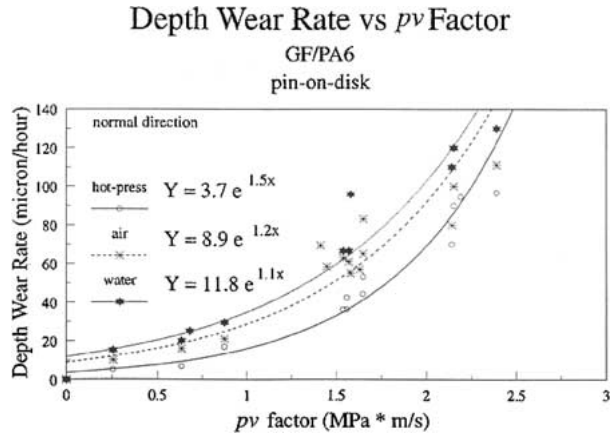

Figure 23 Power regressive relations of wear depth of GF/PA6 pins cooled in three different conditions versus pv factor sliding in normal direction.

$$w_t = ke^{apv}$$

where w_t = depth wear rate (micron/hour), k = wear factor, a = cooling condition factor, p = loading pressure (MPa), v = velocity (m/s).

In this model, the a only related to the microstructures of the composites which were subjected to different cooling conditions in its fabrication. Under a same cooling condition, the a is a constant. However, the k reflected the changes in both cooling condition and sliding direction. In the normal sliding direction, the a and k for different cooled samples are

Hot-press cooled GF/PA6

$$a = 1.5 \quad k = 3.7 \quad Y = 3.7e^{1.5X}$$

Air cooled GF/PA6

$$a = 1.2 \quad k = 8.9 \quad Y = 8.9e^{1.2X}$$

Water cooled GF/PA6

$$a = 1.1 \quad k = 11.8 \quad Y = 11.8e^{1.1X}$$

where $X = pv$ factor in the sliding test (MPa* m/s) and $Y = w_t$ depth wear rate (micron/hour).

The remarkable difference between the three different cooled composites can be seen in the regression lines and in the equations (Fig. 23). For instance, under the same pv conditions, 1 MPa* m/s, the depth wear rate of the hot-press cooled sample was 16.5 μm/hour. The depth wear rate of the hot-press cooled sample was 45% less than the air cooled GF/PA6, and 55% less than the water cooled GF/PA6, respectively. In other words, the pv limit of the hot-press cooled samples was higher than that of air and water cooled samples. Owing to the high thermal stability of the slow cooled samples which is indicated in the last section, it is not difficult to explain the results (Fig. 23).

The pv limit was mainly dependent upon the surface temperature and the polymer thermal decomposition during the sliding test. The sliding surface temperature

was measured by an infrared probe. The temperature in the sliding surfaces at the normal sliding direction appeared about 100°C which was higher than the glass transition temperature of the amorphous nylon matrix, 40°C–50°C, but lower than the melting point of the crystalline nylon matrix, 210°C–226°C. As indicated in a separate paper by the same authors [22] the melting point of the α phase and γ phase were 226°C and 220°C, respectively. The thermodynamical stability of the α phase is higher than that of γ phase. The peak of mechanical loss at a certain temperature decreases with an increase in the α phase crystallinity. The α phase has better dynamical and mechanical properties than that of γ phase at high service temperature. When the sliding surface temperature was above the T_g and below the melting point, the amorphous part of the PA6 matrix behaved like typical rubber, and gave away more easily than the crystalline region. Therefore, the amorphous content of the PA6 matrix was as important as the crystallinity of the α phase for the pv limit. In other words, the crystallinity and T_g of the PA6 matrix have a great effect on the wear rate. The sample with low crystallinity of the α phase, high amorphous contents and low glass transition temperature failed rapidly due to the thermal decomposition and softening.

A slow cooling condition gave the sample a higher crystallinity, larger size of spherulites, more α phase content and higher glass transition temperature than that of fast cooling process. In consequence, it resulted in a higher wear resistance and higher pv limit in the slow cooled samples than that of fast cooled sample.

8. Conclusion

The optimum thermal manufacturing process of the thermoplastic composite bearing materials has been identified. To study the multiple friction and wear mechanisms of fibre reinforced thermoplastic composites in practical applications, a serial of pin-on-disk tests were conducted in this paper. Energy dispersive spectroscopy, X-ray diffraction and scanning electron microscope techniques were used to examine the damage mechanisms of the worn surface, subsurface and worn debris. An infrared probe was used to measure the friction heat in the sliding surfaces.

The effects of the manufacture cooling rate, matrix microstructures and fibre/matrix interface properties on the friction and wear mechanisms have been investigated. Based on the scanning electron microscope analysis of the friction mechanisms, a new friction model was established. Based on a large number of pin-on-disk test results, an empirical wear model was established by using the least square regressing method. The study indicated that

1. The friction coefficient was affected by the cooling rate of the moulding process. The friction coefficient decreased by 7%–14% with decreasing the cooling rate due to the slow cooling gave the composite a strong interfacial bond, and decreased the abrasive friction. Adhesion and abrasion were the main friction mechanisms in the dry continuous pin-on-disk test and interfacial debonding dominated the abrasive friction mechanism. A poor interfacial bond led to more hard particles, glass fibre fragments and a rougher steel surface than that of good interfacial bond. As a consequence, the sliding surfaces were abraded, the oxidative films were damaged, which resulted in a high friction coefficient in the poor interfacial bonding samples.

2. The wear resistance was significantly influenced by the thermal processing of the composite. Decreasing cooling rate during the components thermal moulding would result in an increase of 21%–28% wear resistance when compared with the fast cooling process. The main wear mechanisms were oxidizing wear or thermal decomposition, abrasive wear and adhesive wear in the pin-on-disk test. A slow cooling condition gave the GF/PA6 composite a high crystallinity and high content of the α phase in the PA6 matrix which resulted in a high thermal stability, hard composite, and high adhesive and oxidative wear resistance. A good interface bond contributed to the high abrasive wear resistance as well.

3. Thermal decomposition dominated the pv limit of the GF/PA6 in the pin-on-disk test. A slow cooling gave the GF/PA6 composite pin a high crystallinity, high content of the α phase and high T_g in the PA6 matrix and resulted in a high thermal stability, low wear rate and high pv service limit.

Acknowledgements

Dr. Helen Cartledge would like to thank Dr. Z. F. Zhang for his many valuable discussions through out her first couple years of PhD study. The authors would also like to acknowledge the Australian Postgraduate Research Award for the financial support given to Dr. Helen Cartledge throughout this study and the Toyobo Research Institute, Japan, for providing the GF/PA6 commingled yarn materials used in this study.

References

1. J. BYETT and C. ALLEN, *Tribology International* **25**(4) (1992) 237.
2. H. JACOBI and U. NOWAK, "Advances in Composite Tribology," edited by R. B. Pipes (Elsevier, Amsterdam, 1993) p. 477.
3. U. TEWARI and J. BIJWE, *Composite Materials Series* **8** (1993) 159.
4. K. FRIEDRICH, *ibid.* **8** (1993) 209.
5. F. BILLMEYER, JR., "Textbook of Polymer Science" (John Wiley & Sons, New York, 1984).
6. L. ALEXANDER, "X-ray Diffraction Methods in Polymers Science" (New York, John Wiley & Sons, 1969).
7. M. MATSUO, R. SATO and Y. SHIMIZU, *Colloid & Polymer Science* **271**(1) (1993) 11.
8. N. MURTHY and R. G. BRAY, *Polymer* **36**(20) (1995) 3863.
9. D. HOLMES, C. W. BUNN and D. J. SMITH, *Journal of Polymer Science* **17** (1955) 159.
10. M. KOHAN, "Nylon Plastics" (John Wiley & Sons, New York, 1973).
11. Y. KINOSHITA, *Makromol. Chemistry* **33** (1959) 1.
12. H. ARIMOTO, *Journal of Polymer Science*, A **2** (1964) 2283.
13. H. ARIMOTO, M. ISHIBASHI, M. HIRAI and Y. CHATANI, *ibid.* **3** (1965) 317.
14. H. CARTLEDGE and C. A. BAILLIE, *J. Mater. Sci.* **34**(20) (1999) 5099.
15. *Idem.*, *ibid.* **34**(20) (1999) 5113.
16. L. NIELSEN, *J. Appl. Polym. Sci.* **2**(6) (1959) 351.

17. G. HATFIELD, J. H. GLANS and W. B. HAMMOND, *Macromolecules* **23** (1990) 1654.
18. J. YOO and N. S. EISS, JR., *Wear* **162–164** (1993) 418.
19. K. ILLERS, *Makromol. Chem.* **179** (1978) 519.
20. N. McCRUM, "Anelastic and Dielectric Effects in Polymeric Solids" (John Wiley & Sons, London, 1967) p. 478.
21. Lustinger, 1984.
22. H. CARTLEDGE, C. A. BAILLIE and Y.-W. MAI, *Wear* **194** (1996) 178.
23. F. BOWDEN and D. TABOR, "The Friction and Lubrication of Solids" (Oxford at the Clarendon Press, Oxford, 1964).
24. H. YUMOTO, *Bulletin of Chemistry Society, Japan* **28** (1955) 94.
25. S. SMITH, *Journal of Polymer Science* **30** (1958) 459.
26. I. NOBUYA, "The thermal degradation of nylon six, polyethylene terephthalate and polycarbonate polymers" (University microfilms international, The University of Utah, 1978).
27. T. MIUNOV and A. MAVLYANOV, *Polymer Science, USSR* **12** (1970) 1956.
28. A. SMITH, *Wear* **105** (1985) 91.
29. M. TAKAYANAGI, *Mem. Fac. Eng. Kyushu University* **23**(1) (1963) 1.
30. D. TEER and R. D. ARNELL, "Wear, Principles of Tribology" (The Macmillan Press Ltd, London, 1975) p. 94.
31. H. CZICHOS, *Friction and Wear of Polymer Composites* **s1** (1986) 1.
32. J. SONG, 26th International SAMPE Technical Conference, Oct. 17–20, 1994, p. 627.
33. C. ROWE, *Trans. Am. Soc. Lubric. Engrs* **9** (1966) 100.
34. J. HALLING, "Principles of Tribology" (The Macmillan Press Ltd, London, 1975) eq 5.4, 5.5, p. 101.

Received 17 April
and accepted 11 December 2001